Journal of the Korean Physical Society, Vol. 51, No. 4, October 2007, pp. 1413∼1418

Process Extension Techniques for Optical Lithography: Thermal Treatment, Polarization and Double Patterning

Sang-Kon KIM*
School of Information, Communications and Electronics Engineering, Catholic University of Korea, Bucheon 420-743

Hye-Keun OH†
Department of Applied Physics, Hanyang University, Ansan 426-791

(Received 29 May 2007, in final form 6 July 2007)

Current 193-nm optical lithography and commercially available 193-nm resists have been pushed far beyond the previously expected critical dimension by using process extension technology for resolution enhancement technology. This paper deals with three kinds of process extension technologies, thermal treatment, polarization, and double patterning. These technologies are modeled and analyzed. If a 50 % pattern shrinkage due to thermal treatment, a 25 % resolution enhancement due to polarization, and a 50 % pattern shrinkage due to double patterning are supposed, an effective combination can generate a sub-50-nm pattern. When the pattern size is smaller, optical proximity effects are more severe. After describing optical proximity effects for each of these technologies, we discuss optical proximity correction methods.

PACS numbers: 85.40.Hp, 78.20.Bh, 85.40.Bh
Keywords: Lithography, Lithography simulation, Thermal treatment, Polarization, Double patterning

I. INTRODUCTION

From the Rayleigh equation, $R = k_1 \times \lambda/NA$, resolution ($R$) improvement methods without wavelength (λ) reduction reduce the process difficulty level (k_1) and increase the numerical aperture (NA). As those resolution enhancement methods, three kinds process technologies, thermal treatment, polarization, and double patterning, have been researched. For efficient applications, those technologies, must be modeled and analyzed so as to be able to control them. In the lithography process, thermal processes are dealt with by using softbake (SB), post-exposure bake (PEB), and thermal reflow. Those three kinds of thermal processes are the same thermal process, but have different effects on the critical dimension. If the k_1 factor is almost at the theoretical limit with the current 193-nm ArF wavelength, the only remaining way to increase the resolution may be by increasing the numerical aperture (NA) way. However, as the NA is increased, imaging contrast becomes worse in terms of polarization effects. TE mode (or s-polarized) illumination has been proposed to increase the contrast of high-NA imaging. Double patterning splits a design layer into two design layers and performs double lithography and etch processes.

*Corresponding Author: sangkona@hotmail.com;
†E-mail: hyekeun@hanyang.ac.kr

The current status of lithography technologies for resolution in half pitch is shown as empty squares in Figure 1(a). Lin predicts a pattern reduction, filled squares of Figure 1(a), by using high-index materials, polarized illumination, a solid-immersion mask, and a split-pitch technique (or double patterning) [1]. Figure 1(b) shows the relation between k_1 and NA for the 193-nm wavelength according to the Rayleigh equation. When NA is 0.6 (or 0.95) and k_1 is 0.3, a half-pitch pattern of 96.5 (or 60.94) nm is formed. When k_1 is 0.3 and NA is 1.35, the manufacture of semiconductors with a half-pitch pattern of 42.8-nm is possible. For a half-pitch formation of 25-nm and a NA of 0.6 (or 0.95), k_1 must be 0.077 (or 0.123), which is beyond the ideal-limit value of 0.25. In this paper, three kinds of extension technologies are described, modeled, and analyzed by increasing the NA and decreasing k_1.

II. THERMAL TREATMENT

Thermal treatment is a thermal process using current-day lithography equipment and chemically amplified resists (CARs). The SB process is used to remove excess solvent after spin coating, to relieve strain in the solid film, and to provide better adhesion to the substrate. During SB, the free volume content of a photoresist significantly affects its lithographic properties. PEB is used

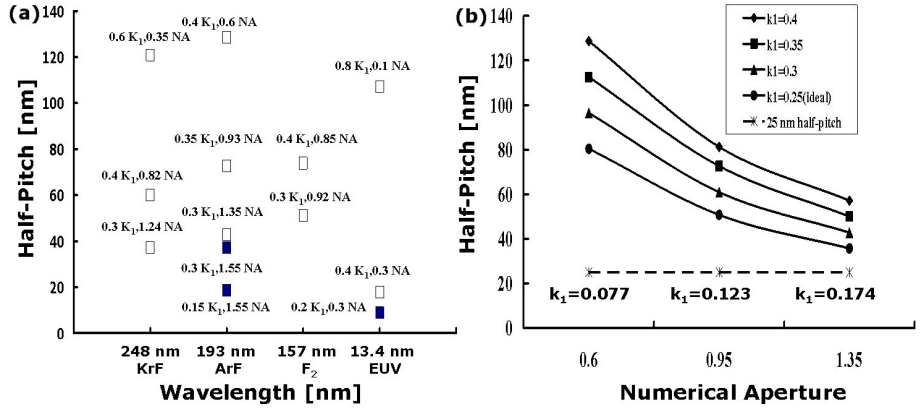

Fig. 1. Graph of half-pitch due to Rayleigh parameters of lithography technologies in the (a) current status and at a (b) 193-nm wavelength.

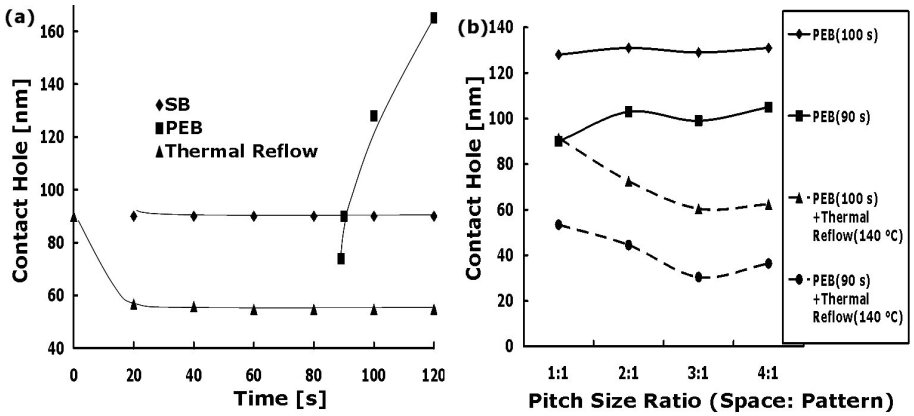

Fig. 2. Simulation results of (a) reduced performance due to thermal processes in the 3 × 3 array pattern of a 90-nm contact hole and (b) the dependence of the size of the contact hole on the pitch size as obtained by using the PEB time with the optical proximity correction and thermal reflow.

to reduce the standing wave effect. Exposing the resist to deep ultraviolet (DUV) light generates acid from the photoacid generator (PAG). During a subsequent PEB, the acid diffuses from an exposed region to an unexposed region washing out standing waves and causing the reacted region to be larger than the initially exposed region. In addition, most CARs exhibit volume shrinkage after the PEB step due to desorption of volatile byproducts created during the bake. Thermal reflow is used to reduce the pattern size by using thermal heating at temperatures above the glass transition temperature of the resist after development. When the resist is heated to a temperature above its glass transition temperature, the bonding of the synthesized resist is reduced, and its mobility is improved. The three-dimensional structure of the synthesized resist is changed, and the contact hole (C/H) is shrunk due to the additional thermal energy.

Figure 2(a) shows the simulation results obtained for reduced performances for a 90-nm 3 × 3 C/H and dense 1 : 1 array pattern in thermal processes by using a homemade tool [2]. For a C/H, critical dimension (CD) dose not changed due to SB time, so that SB time is not an effective parameter. When the time of the PEB is increased, the C/H is larger, so that an underbake can reduce the C/H size. Thermal reflow reduces a 90-nm C/H to a 55-nm C/H. In the active area of Figure 2(a), in which the CD depends on time, the sensitivity of the CD to the PEB time (2.5 nm/s), the slope of the CD vs. PEB time, is larger than that of thermal reflow time (2.2 nm/s). Figure 2(b) shows that the simulation results for the C/H depend on the pitch sizes which are obtained by using PEB time and thermal reflow, The solid lines in Figure 2(b) show the size of the contact hole as a function of the pitch size ratio of a 140 nm 3 × 3 C/H mask pattern for PEB times of 100 s and 90 s. Those patterns can be reduced to the C/H patterns with sizes between 53 and 36 nm, the dot line of Figure 2(b) with circles, by using a PEB time of 90 s and a thermal reflow of 140 °C. However, as the patterns in Figure 2(b) vary with the pitch size ratio, the optical proximity effects (OPEs) of the reduced PEB time and thermal reflow cannot be neglected. The OPEs are quite severe as the critical dimensions shrink down to a 25-nm half-pitch, so it is important to define the OPEs and to develop

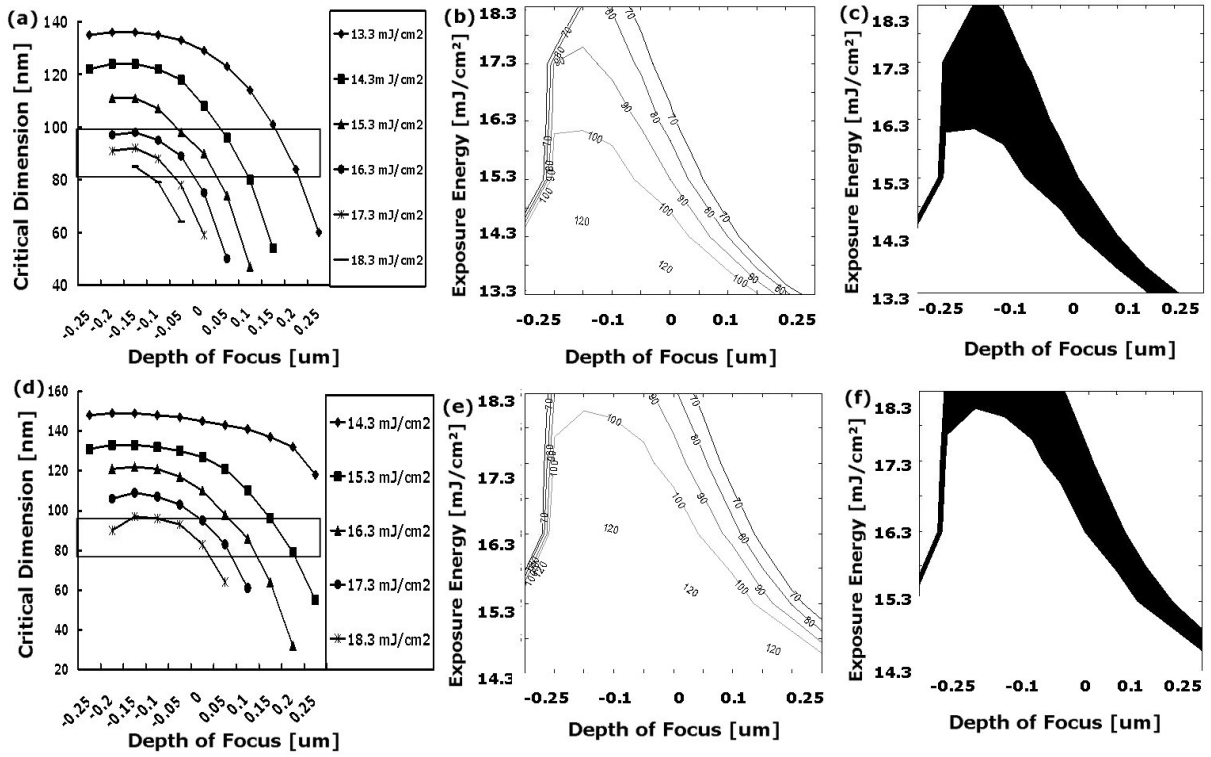

Fig. 3. Simulated results of TE and TM polarizations in Bossung curves of the focus and the exposure: (a) and (d) critical dimension for TE and TM, respectively, as a function of the depth of focus, exposures as function of the depth of focus for (b) TE and (e) TM, and the process windows of a 90-nm CD (nominal ±10 %) for (c) TE and (f) TM.

the optical proximity correction (OPC) to compensate for the OPEs. Those thermal processes have similar effective parameters, such as the baking temperature, the baking time, the original characteristics of the resist, the surrounding resist volume, the initial pattern′s size and shape, and the pattern array. In terms of Figure 2, the thermal reflow bias can be represented as

$$\Delta CD = CD_{before} - CD_{after} = f\left(t_b, T_b, V_n, K_r\right), \quad (1)$$

where CD_{before} is the critical dimension before thermal reflow, CD_{after} is the critical dimension after thermal reflow, t_b is the baking time, T_b is the baking temperature, V_n is the resist volume surrounding the pattern related with pitch, and K_r is the resist′s original characteristics [1,4]. From the experimental results for thermal reflow in Ref. 5, the thermal reflow bias can be modified, by using Eq. (1), as

$$\begin{aligned}\left(\Delta CD\right)^2 &= f\left(T_b\right)\cdot f\left(V_n\right)\\ &= \left[\alpha_1\cdot\exp\left(\alpha_2/T\right)\right]\left[\alpha_3\cdot\exp\left(\alpha_4\mathcal{R}\right)\right]\\ &= \left[3.696\times10^{29}\cdot\exp\left(-8347.64393/T\right)\right]\\ &\times\left[1.88152\cdot\exp\left(-1.90217\cdot\mathcal{R}\right)\right], \end{aligned} \quad (2)$$

where the resist′s original characteristics K_r are ignored and the ratio ($\mathcal{R}$) of the contact hole to the half-pitch size is used instead of the resist volume V_n.

III. POLARIZATION

For hyper-NA systems, the vector nature of light cannot be neglected, and a vector diffraction theory is clearly needed to account for the inherent coupling between the vector components and the polarization of the electromagnetic filed [6]. In an optical lithography imaging system, polarization can be distinguished into source polarization, mask polarization, and projection lens polarization, such as lens pupil polarization. If two plane waves interfere completely, the total TE intensity

$$I_{TE} = |\vec{E}_1 + \vec{E}_2|^2 = |\vec{E}_1|^2 + |\vec{E}_2|^2 + 2|\vec{E}_1||\vec{E}_2|. \quad (3)$$

If the angle between the two plane waves is 2θ in the TM polarization [7], the geometric projection of the electric field vector $\vec{E}_2$ in the same direction as $\vec{E}_1$ is $\vec{E}_2\cos(2\theta)$. The TM intensity is given by the coherent sum of the parts that overlap plus the incoherent sum of the parts that don't overlap:

$$\begin{aligned} I_{TM} &= |\vec{E}_1 + \vec{E}_2\cos(2\theta)|^2 + |\vec{E}_2\sin(2\theta)|^2\\ &= |\vec{E}_1|^2 + |\vec{E}_2|^2 + 2|\vec{E}_1||\vec{E}_2\cos(2\theta)|. \end{aligned} \quad (4)$$

By using the Rayleigh equation ($R = k_1\times\lambda/NA$), if $|\vec{E}_1| = |\vec{E}_2| = 1$, the contrasts of the TE and the TM polarizations are

$$TEcontrast = \frac{I_{max} - I_{min}}{I_{max} + I_{min}}$$

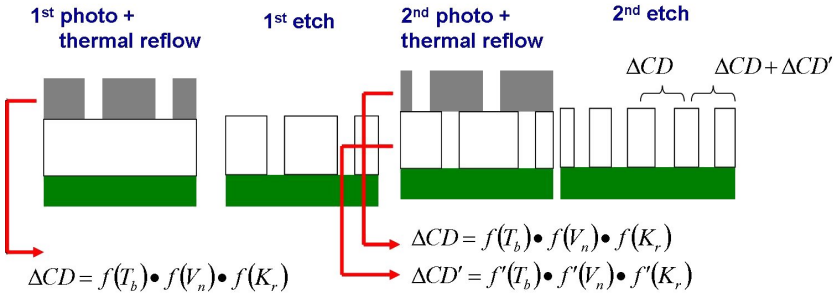

Fig. 4. Double patterning of C/H with thermal reflow included.

$$= \frac{|\vec{E}_1+\vec{E}_2|^2-|\vec{E}_1-\vec{E}_2|^2}{|\vec{E}_1+\vec{E}_2|^2+|\vec{E}_1-\vec{E}_2|^2} = \frac{4|\vec{E}_1||\vec{E}_2|}{2\left(|\vec{E}_1|^2+|\vec{E}_2|^2\right)} = 1, \tag{5}$$

$$TM contrast = \frac{I_{max}-I_{min}}{I_{max}+I_{min}}$$
$$= \frac{|\vec{E}_1+\vec{E}_2|^2-|\vec{E}_1-\vec{E}_2|^2}{|\vec{E}_1+\vec{E}_2|^2+|\vec{E}_1-\vec{E}_2|^2} = \frac{4|E_1||E_2\cos(2\theta)|}{2\left(|E_1|^2+|E_2|^2\right)}$$
$$= \cos(2\theta) = 1-2\sin^2\theta = 1-2\left[\frac{k_1\lambda}{n\cdot R}\right]^2, \tag{6}$$

where k_1 is a process constant, λ is the wavelength, n is the refractive index, and R is the half pitch. When the pattern size is small, the TM polarization effect on the contrast of the aerial image is more severe according to Eq. (6).

Figure 3 shows the simulated results of TE and TM polarization in Bossung curves of the focus and exposure: (a) and (b) critical dimensions for TE and TM, respectively, as a function of the depth of focus, exposures as functions of the depth of focus for (b) TE and (e) TM, and the process windows of a 90-nm CD (nominal ±10 %) for (c) TE and (f) TM. Simulation conditions are a 193-nm wavelength, a 0.8 NA, and a dipole (radius: 0.5, hole size: 0.3, angle: 45) for a 90-nm line and space (L/S). The rectangular box in Figure 3(a) is a ±10 % range for a 90-nm pattern. The rectangular box of the TE Bossung curve of Figure 3(a) includes more exposure graphs than that of the TM Bossung curve in Figure 3(d), so the TE polarization has a larger process window than the TM polarization. For a 90-nm pattern, the target exposures of the TE and the TM are 15.3 mJ/cm^2 and 17.5 mJ/cm^2, respectively. The process latitude can be calculated as the number of exposure conditions within a process window, which is the rectangular box in Figure 3(a) or the black area in Figure 3(c). The TE polarization in Figure 3(c) has the 25 % larger process latitude of percent exposure variation and depth of focus (DOF) than the TM polarization in Figure 3(f). As the process latitude is directly proportional to resolution enhancement, the TE polarization can be assumed to have a 25 % resolution enhancement.

IV. DOUBLE PATTERNING

For small pattern formation, dense pattern formation is more difficult than sparse pattern formation. Double patterning is a method of splitting the mask pattern into larger pitches to delineate them separately and without cross-exposure interference onto the same areas on the wafer.

Figure 4 shows the double patterning of a C/H with thermal reflow. The C/H pattern in the final image is split into two layers at more relaxed pitch. The first step consists of patterning a small semi-isolated trench at this more relaxed pitch. After the etching and thermal reflow in this first layer, we used an identical second exposure. The shrinkage of the thermal reflow at the more relaxed pitch is larger than at a dense pitch because the thermal reflow bias depends on the resist volume surrounding the C/H. However, a second thermal reflow bias can be produced in the first layer after the second thermal reflow. When the time of thermal reflow is constant, the thermal reflow bias can be defined, according to Eq. (1), as

$$\Delta CD = CD_{before} - CD_{after} = f(T_b, V_n, K_r)$$
$$= f(T_b)\cdot f(V_n)\cdot f(K_r), \tag{7}$$

where the baking temperature T_b, the resist volume V_n, and the resist's original characteristics K_r are independent of each other. The second thermal reflow bias can be defined as

$$\Delta CD' = CD'_{before} - CD'_{after} = f'(T_b, V_n, K_r)$$
$$= f'(T_b)\cdot f'(V_n)\cdot f'(K_r). \tag{8}$$

Hence, the final thermal reflow biases of the first layer and the second layer are $\Delta CD + \Delta CD'$ and ΔCD, respectively. Although the bias of the first layer in the second thermal reflow is smaller than that in the first thermal reflow, the thermal effects of the second thermal flow are considered to form uniform, repeated patterns by using the baking temperature T_b and the resist volume V_n. The double patterning of thermal reflow can be applied not only to C/H patterns but also to line and space (L/S) patterns [8]. After the small sparse spaces are made by using thermal reflow, dense L/S patterns can be formed through double patterning. Overlay of

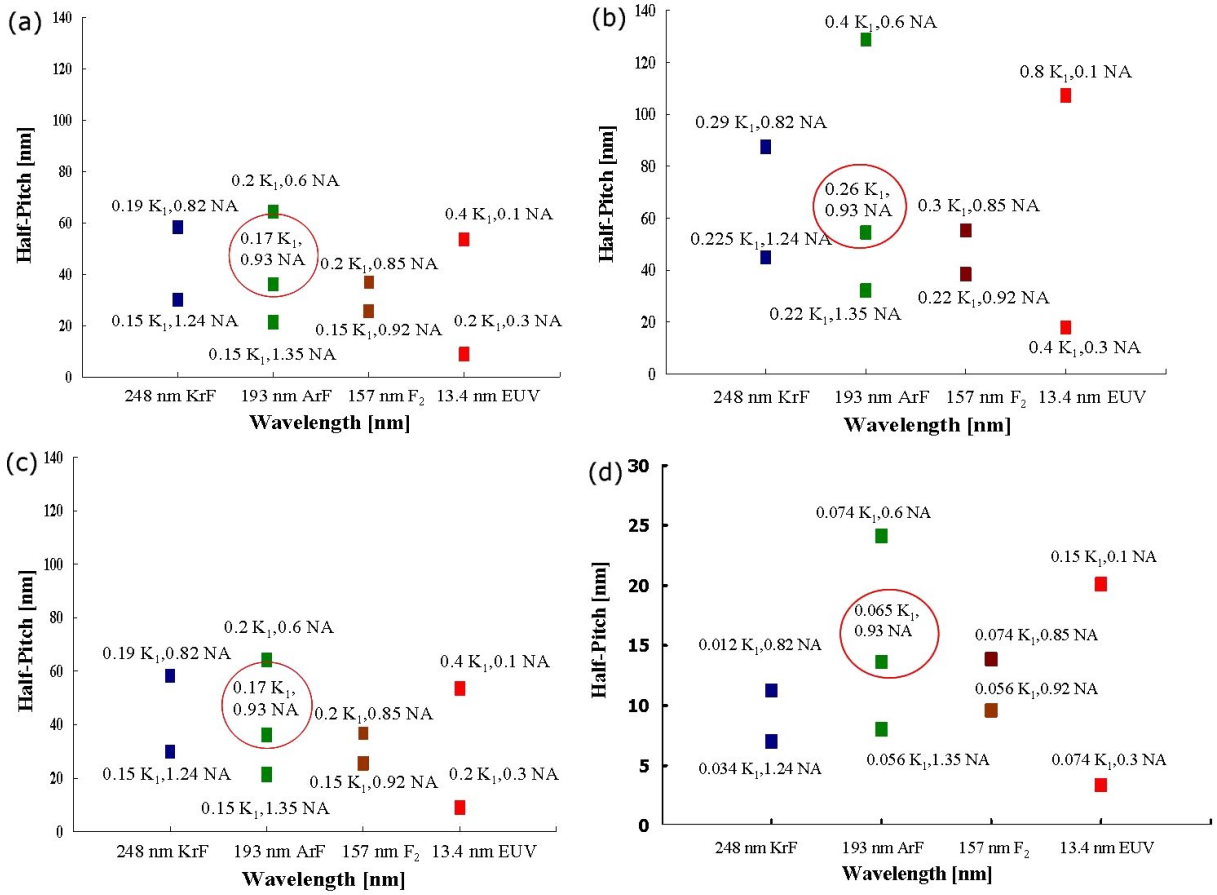

Fig. 5. Calculated pattern shrinkage from the current lithography status in Figure 1(a) due to the three kinds of process technologies, (a) thermal treatment, (b) polarization, (c) double patterning, and due to (d) a combination of the three technologies.

the first and the second layers is the most critical problem in the double patterning technique. However, an appropriate use of the mask design can reduce the critical problem of the alignment of the second exposure [1].

V. ANALYSIS

Figure 5 shows the simulated pattern shrinkage from the current lithography status in Figure 1(a) due to the three process technologies, thermal treatment, polarization, and double patterning. A 50 % pattern shrinkage for thermal treatment, a 25 % resolution enhancement for polarization, and a 50 % pattern shrinkage for double patterning are possible. For a 60.94-nm pattern with a 0.93 NA and a 193-nm ArF wavelength, the circles in Figure 5 show half pitches of 35.28-nm due to thermal treatment (Figure 5(a)), 53.96-nm due to polarization (Figure 5(b)), 35.28-nm due to double patterning (Figure 5(c)), and 13.6-nm due to a combination of the three technologies (Figure 5(d)). Both thermal treatment and double patterning can cause the largest shrinkage among those technologies. However, double patterning has the lowest yield because the yield is related to the number of process steps. Therefore, the high-yield technology of the double pattering is required.

VI. CONCLUSION

As process extension technology for current lithography, thermal treatment, polarization, and double patterning were modeled and analyzed. A 50 % pattern shrinkage for thermal treatment, a 25 % resolution enhancement for polarization, and a 50 % pattern shrinkage for double patterning are possible. A combined thermal reflow and double patterning technology is described for the possibility of sub-50-nm pattern formation. Since optical proximity effects are severe in small patterns, optical proximity correction methods are discussed for each of the technologies. Those three technologies extend the current technology, so that we recommend that those technologies be developed with a new generation lithography system.

ACKNOWLEDGMENTS

This work was supported by the Korea Research Foundation Grant funded by the Korean Government (MOEHRD, Basic Research Promotion Fund) (KRF-2006-331-D00306).

REFERENCES

[1] B. J. Lin, Microelectronic Eng. **83**, 604 (2006).
[2] S.-K. Kim, J. Korean Phys. Soc. **49**, 1211 (2006).
[3] S.-K. Kim, H.-K. Oh, I. An, S.-M. Lee, C.-K. Bok and S.-C. Moon, J. Korean Phys. Soc. **46**, 1439 (2005).
[4] S.-K. Kim and H.-K. Oh, J. Korean Phys. Soc. **47**, S377 (2005).
[5] S.-K. Kim, Jpn. J. Appl. Phys., **45**, 5400 (2006).
[6] S.-K. Kim and H.-K. Oh, J. Korean Phys. Soc. **41**, 456 (2002).
[7] M. McCallum, G. Fuller and S. Owa, Microelectronic Eng. **83**, 667 (2006).
[8] H.-R. Kim, Y.-B. Ahn, J. Kim, S. Kim, D. Park and Y.-S. Kim, SPIE **6154**, 615441 (2006).